RSC Advances

PAPER

Check for updates

Cite this: *RSC Adv.*, 2023, **13**, 6954

Hybrid carbonaceous adsorbents based on clay and cellulose for cadmium recovery from aqueous solution

Leila Azaryouh,[ab] Hajar Abara,[c] Zineb Kassab,*[a] El-houssaine Ablouh,*[a] Adil Aboulkas,[b] Mounir El Achaby[a] and Khalid Draoui*[c]

The current work describes the synthesis of carbonaceous composites *via* pyrolysis, based on CMF, extracted from Alfa fibers, and Moroccan clay ghassoul (Gh), for potential use in heavy metal removal from wastewater. Following synthesis, the carbonaceous ghassoul (ca-Gh) material was characterized using X-ray fluorescence (XRF), Scanning Electron Microscopy coupled with Energy Dispersive X-ray (SEM-EDX), zeta-potential and Brunauer–Emmett–Teller (BET). The material was then used as an adsorbent for the removal of cadmium (Cd^{2+}) from aqueous solutions. Studies were conducted into the effect of adsorbent dosage, kinetic time, initial concentration of Cd^{2+}, temperature and also pH effect. Thermodynamic and kinetic tests demonstrated that the adsorption equilibrium was attained within 60 min allowing the determination of the adsorption capacity of the studied materials. The investigation of the adsorption kinetics also reveals that all the data could be fit by the pseudo-second-order model. The Langmuir isotherm model might fully describe the adsorption isotherms. The experimental maximum adsorption capacity was found to be 20.6 mg g^{-1} and 261.9 mg g^{-1} for Gh and ca-Gh, respectively. The thermodynamic parameters show that the adsorption of Cd^{2+} onto the investigated material is spontaneous and endothermic.

Received 28th December 2022
Accepted 17th February 2023

DOI: 10.1039/d2ra08287j

rsc.li/rsc-advances

1. Introduction

All life on Earth depends on water, a renewable natural resource; due to overuse and contamination, fresh water is becoming increasingly rare.[1] Worldwide, water contamination causes illness and numerous deaths.[2] It is an issue in both developed and developing nations. The main threat to water quality are activities like mining, urban development, and agriculture.[3] Pollutants can have a variety of sorts and characteristics such as non-biodegradable polymers synthetic chemicals, organic and inorganic dyes, and heavy metals, which have no or very little adsorptive potential.[4] These contaminants build up in the environment over time, as their number or quantity grows, so does their harm. It has been reported that oral exposure to heavy metals such as Cd has been found to target organ toxicity, including unfavourable health effects on neurological, reproductive, cardiovascular, gastrointestinal, renal, musculoskeletal, and cutaneous systems.[5,6] Cd ions are produced in large quantities by industries such as ceramics, batteries, metallurgy, electroplating as well as mining.[7] The concentration of this hazardous heavy metal must therefore be eliminated or reduced in the aquatic environment. Several treatment methods, including adsorption, membrane separation,[8] coagulation–flocculation,[9] osmosis,[10] and chemical precipitation[11] have been used to get rid of harmful metal ions. Adsorption is a common treatment method because it is affordable, easy to use, and especially environmentally friendly.[12–15] In this context, more efficient approach must be investigated instead of the more popular typically expensive treatment methods. Clay has been the subject of various studies in order to develop potential adsorbents.[16–18] One of the clays that caught the interest of researchers was ghassoul. It is an abundant Moroccan stevensite and its use in water treatment applications was the subject of numerous investigations.[16,19] It was mentioned that stevensite can exchange the cations stored in its aluminosilicate structure for cations from an external solution through the process of ion exchange.[20] The effectiveness of Ghassoul in adsorbing malachite green and basic yellow 28 from an aqueous solution is already discussed in the literature.[21] Another study looked at this Moroccan clay's ability to remove cationic dye from aqueous solution.[22] Ghassoul has also proved its potential in removing heavy metals.[23–25] On the other side, the use of variety of biopolymers for the removal of heavy

[a]*Materials Science, Energy, and Nano-Engineering (MSN) Department, Mohammed VI Polytechnic University (UM6P), Lot 660 – Hay Moulay Rachid, Benguerir, 43150, Morocco. E-mail: elhoussaine.ablouh@um6p.ma; zineb.kassab@um6p.ma*

[b]*Equipe des Procédés Chimiques et Matériaux Appliqués (EPCMA), Faculté Polydisciplinaire de Béni-Mellal, Université Sultan Moulay Slimane, BP 592, 23000 Béni-Mellal, Morocco*

[c]*Laboratory of Materials and Interfacial Systems, Faculty of Sciences-Tetouan-Abdelmalek Essaadi University (UAE), P. B. 2121, 93000 Tétouan, Morocco. E-mail: khdraoui@gmail.com*

This article is licensed under a Creative Commons Attribution-NonCommercial 3.0 Unported Licence.

© 2023 The Author(s). Published by the Royal Society of Chemistry

metals as adsorbent from wastewater has also attracted great attention. Due to their affordability, effectiveness and biodegradability, lignin, cellulose, chitin and alginate-based adsorbents have been employed widely, as it's the case in those research.[26–30] Those biopolymers have a variety of functional groups which improve the effectiveness of removing heavy metals from water samples.[31–35] Cellulose can be found in wood and cotton; however, many other resources have been investigated to resolve environmental concerns.[28,36,37] Dong Shen Tong *et al.* reported in their work[38] that recently, a new class of adsorbents has emerged, consisting of carbonaceous materials with numerous oxygen-containing functional groups anchored on the surface of solid surface. The challenges produced by excessive levels of pollution demonstrate the necessity of research to reduce the damage. The quest for solids that function as highly polluting heavy metals is an ongoing activity in the context of adsorption. Finding low-cost, abundant, and environmentally friendly adsorbents is essential. To our knowledge, no research has previously been done on the potential for cellulose and ghassoul combined to create a low-cost adsorbent material. Therefore, this combination could be very interesting by providing better adsorbent qualities such as a larger surface area, higher adsorption efficiency. One of the primary goals of investigating a contaminant's adsorption process is to determine the optimum operating parameters. Numerous studies were conducted to identify the quantities or values required for the various factors to achieve optimal removal efficiency. pH, temperature, contact time, adsorbent mass, and adsorbate concentration are among the characteristics considered. In this work, pyrolysis will be used for the synthesis of a novel material based on ghassoul combined with cellulose. The created material will be fully characterized using a variety of techniques. Also understanding the behaviour of the adsorbent toward cadmium ions in aqueous solutions is going to be investigated by varying various experimental conditions.

2. Materials and methods

2.1. Materials

The clay used in this work was a commercial ghassoul (Gh), washed with distilled water, dried, milled and sieved in a stainless-steel sieve of diameters of 300 μm, then it was used for synthesis of the composite materials. Raw Alfa Fibers (Stipa Tenacissima plant) (RF) used in this work were collected from the oriental region of eastern Morocco. Cadmium sulfate ($CdSO_4$) and the chemicals used for the cellulose micro-fibers (CMF) extraction were all purchased from Sigma-Aldrich.

2.2. Extraction of cellulose microfibers and preparation of the carbonaceous composite

CMF were extracted from Raw Alfa fibers (RF) through an alkali treatment followed by a bleaching process. For the alkali treatment, the ratio of fibers to liquor was 1 : 20 (g mL^{-1}), the grind RF were treated once with 10 wt% NaOH solution at 80 °C for 2 hours under mechanical stirring giving rise to ATF. ATF were followed by a bleaching treatment which was carried out using a solution made up of equal parts (v/v) of acetate buffer (27 g NaOH and 75 mL glacial acetic acid, diluted to 1 L of distilled water) and aqueous sodium chlorite (1.7 wt% $NaClO_2$ in water). This treatment was done once for 2 hours at 80 °C under mechanical stirring, resulting in white CMF. The first step of the synthesis of the carbonaceous composite was the mixing of the two materials, for that we used solution mixing technique. As shown in the Fig. 1, a distinct quantity of 7.5 g of the extracted CMF was well dispersed in distilled water for several minutes, followed by the addition of 22.5 g of Gh to the mixture. After two hours of continuous magnetic stirring, the solution was freeze at −80 °C then dried by a freeze drier for 48 hours. The freeze-drying method has been chosen in order to ensure the adherence and the good dispersion of the fibers with

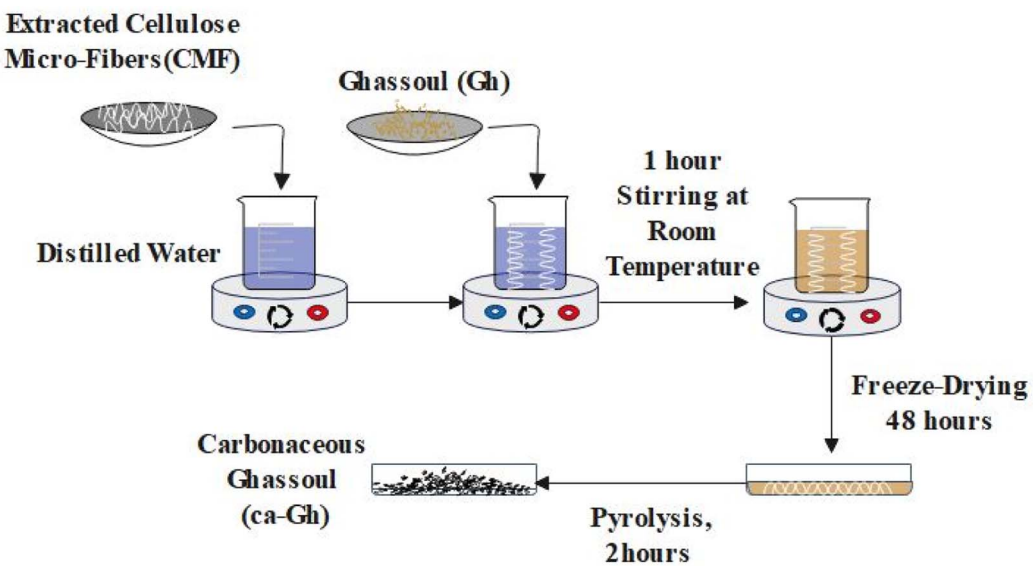

Fig. 1 Schematic representation of the synthesis of ca-Gh.

© 2023 The Author(s). Published by the Royal Society of Chemistry

the clay. Right forward, the pyrolysis process was carried out for two hours straight at 700 °C under argon (5°C min^{-1}). 19.39 g of carbonaceous ghassoul (ca-Gh) was obtained after pyrolysis.

2.3. Characterization techniques

Fourier transform infrared spectra (FTIR) was used to identify the functional groups present in the samples using PerkinElmer Spectrum 2000 FTIR. The experiments were carried out in the range of 4000 to 600 cm^{-1} and an accumulation of 16 scans. Bruker diffractometer was used in this work to identify the crystalline structure of the samples using a monochromatic CuKα radiation at $\lambda = 1.54056$ Å in the range of $2\theta = 5°–40°$ with a scanning rate of 2° min^{-1}. The crystallinity index (CrI) was calculated using the Segal equation from the XRD data:

$$\mathrm{CrI} = \frac{I_{200} - I_{\mathrm{am}}}{I_{200}} \times 100 \quad (1)$$

where I_{200} refers to the principal intensity of the crystalline portion of cellulose and I_{am} is the intensity of the amorphous portion of cellulose and other constituents.

The basal spacing of the clay was calculated according to the Bragg equation:

$$d_{001} = \frac{1.54}{2\sin(\theta)} \quad (2)$$

where θ represents the incident angle and d_{001} stands for the clay basal spacing.

The chemical composition of the clay was determined by X-ray fluorescence spectrometry (XRF) using Malvern Panalytical Epsilon 4 dispersive spectrometer. Discovery TGA, TA instruments, was used to evaluate the thermal stability of the materials. 5–10 mg of the samples were heated to 700 °C under a nitrogen atmosphere at a heating rate of 10 °C min^{-1}. Zeiss Evo 10 scanning electron microscopy (SEM) connected to an Energy Dispersive X-ray spectroscope (EDX) was used to examine the morphology of the materials and to determine the elements on the surface of the samples. The sample's surface was coated with a thin conductive gold layer using sputtering apparatus. GEMINI VII 2390 Instrument was used to measure the specific surface area and also adsorption/desorption isotherm (BET) of the samples using the adsorption of N_2 at the temperature of liquid nitrogen, the materials were both degassed at 200 °C for 12 hours before the analysis. For the zeta potential measurement, a 1 g L^{-1} clay suspension after two minutes of sonication was stirred for 1 hour long. After decantation, the zeta potential is determined from the supernatant using Malvern Zetasizer Nano ZS.

2.4. Adsorption study

ca-Gh adsorbent was tested for its adsorption efficiency of cadmium ions (Cd^{2+}) in response to the initial Cd^{2+} concentration, stirring time, temperature, masse of the adsorbent and pH of the medium effect. For this purpose, 15 mg of the adsorbent was added to a container containing 15 mL of 100 mg L^{-1} of Cd^{2+} solution. The containers were stirred at room temperature and then the solution is analysed using an atomic absorption spectrometer (Agilent Technologies 200 Series AA). The amount of Cd^{2+} ions adsorbed per gram of adsorbent (q_e) was calculated using the following equation:

$$q_e = \frac{(C_0 - C_e) \times V}{m} \quad (3)$$

where C_0 stands for initial concentration of Cd^{2+} (mg L^{-1}), C_e: Cd^{2+} concentration at equilibrium time (mg L^{-1}), m: dry adsorbent's mass (g) and V: total volume of suspension (L).

2.4.1. Temperature effect. Different thermodynamic parameters were investigated in order to analyse and understand the adsorption process. For this study, the temperature of the experience varied from $T = 25$ °C to $T = 40$ °C. The Van't Hoff equation was used to determine the thermodynamic parameters, including the changes in standard enthalpy (H), standard entropy (S), and standard free energy (G).[39]

$$\ln K = -\frac{\Delta G°}{RT} = -\frac{\Delta H°}{RT} + \frac{\Delta S°}{R} \quad (4)$$

T is the solution's temperature (K), K represents the equilibrium constant or linear adsorption distribution coefficient, and R refers to the gas constant ($R = 8.314$ J (mol^{-1} K^{-1})). $\Delta H°$ and $\Delta S°$ are calculated from the slope and intercept of the plot of ln K *vs.* $1/T$, respectively.

2.4.2. Kinetic and equilibrium modelling. For the kinetic study, the mass of the adsorbent and the concentration of Cd^{2+} was kept constant, $m = 15$ mg and $C_i = 100$ mg L^{-1}, respectively, while varying the time from $t = 30$ min to $t = 360$ min. To evaluate the efficiency of ca-Gh in removing Cd^{2+} ions and to determine the mechanisms of the adsorption process, the experimental data were fitted using two kinetic models: pseudo-first-order (eqn (5)) and pseudo second-order (eqn (6)) models.[40] q_t (mg g^{-1}) and q_e (mg g^{-1}) stand for the amount of Cd^{2+} adsorbed at t time and equilibrium time, respectively. For pseudo-first-order and pseudo-second-order kinetic models, K_1 and K_2 are the rate constant, respectively.

$$\log(q_e - q_t) = \log q_e - k_1 t \quad (5)$$

$$\frac{t}{q_t} = \frac{1}{k_2 {q_e}^2} + \frac{1}{q_e} t \quad (6)$$

For the isotherm investigation, the only parameter that was varying is the initial concentration of Cd^{2+}, from $C = 20$ mg L^{-1} to $C = 600$ mg L^{-1}. Langmuir (eqn (7)) and Freundlich (eqn (8)) models were used to investigate the isotherms data.[41] In terms of adsorption capacity, q_e is the maximum Cd^{2+} uptake per mass of the adsorbent (mg g^{-1}), K_L is the Langmuir constant (L mol^{-1}), which is related to the energy of the adsorption, K_F is the Freundlich constant, and n describes the adsorption intensity.

$$q_e = \frac{K_L q_m C_e}{1 + K C_e} \quad (7)$$

$$q_e = K_F {C_e}^{1/n} \quad (8)$$

© 2023 The Author(s). Published by the Royal Society of Chemistry

3. Results and discussion

3.1. Characterization

3.1.1. Cellulose microfibers characterization. The extraction yield from RF to ATF was found to be 48.46%, and from ATF to CMF, the yield is 82.51%. The chemical composition and the surface functionality of materials at different phases of the treatment were investigated using FTIR spectroscopic technique. Fig. 2(a) shows the FTIR spectra of RF, ATF, and CMF. The broad peaks observed at 3370–3250 cm^{-1} are attributed to hydroxyl groups O–H and aliphatic C–H stretching vibrations present in lignocellulosic materials.[42,43] The peaks at 1511 cm^{-1} and 1246 cm^{-1} correspond to the C=C stretching vibration from the aromatic ring and C–O–C out of plane stretching vibration of the aryl group in lignin and hemicelluloses. The peak at 1729 cm^{-1} can be assigned to the acetyl and uronic ester groups of hemicellulose or the ester linkage of carboxylic group of fluoric and *p*-coumaric acids of lignin and/or hemicellulose.[44] As it can be noticed, the mentioned peaks were not detected in the treated fibers spectra, which can suggest the successful removal of the lignin and hemicellulose after the alkali and bleaching treatment. The peak at 2927 cm^{-1} and 2840 cm^{-1} are assigned to methylene group and symmetric stretch of CH_3 of methoxyl group respectively. The peak detected at 1633 cm^{-1} is caused by the bending mode of the adsorbed water.[42] The peak at 1159 cm^{-1} corresponds to C–O–C asymmetric stretching of the cellulose as was reported in this work.[42] The gradual increasing intensity of the mentioned peak indicates that the cellulose content was increased after the alkali and bleaching treatment.[44]

Fig. 2(b) shows the XRD profile of the raw and treated fibers. From this result, it can be noticed that all cellulosic materials show distinctive peaks of the cellulose crystalline structure type I around 14.9°, 16.3° and 22.5°, corresponding to the crystallographic planes at 1$\bar{1}$0, 110 and 020, respectively.[42] As it was expected, after the chemical treatment, the magnitude of the observed crystalline peaks increased, which is due to the removal of amorphous lignin and hemicellulose. It is noteworthy to notice that the crystal structure of the cellulosic component was not altered throughout the alkali and bleaching treatment. The crystallinity index (CrI) was found to be about 58%, 79% and 82% for RF, ATF and CMF samples, respectively. The increase of CrI as the process goes on confirms the elimination of the amorphous phases.[45]

As mentioned in the literature, the thermal decomposition of lignocellulosic materials starts at a lower temperature for hemicellulose in general, followed by an early stage of degradation of lignin molecules, and then by the decomposition of cellulose.[46] It can be noticed from the results presented in Fig. 2(c) and (d). Due to the hydrophilic nature of the cellulosic materials, all the samples show a small weight loss of around 100 °C due to the evaporation of absorbed moisture.[47] RF

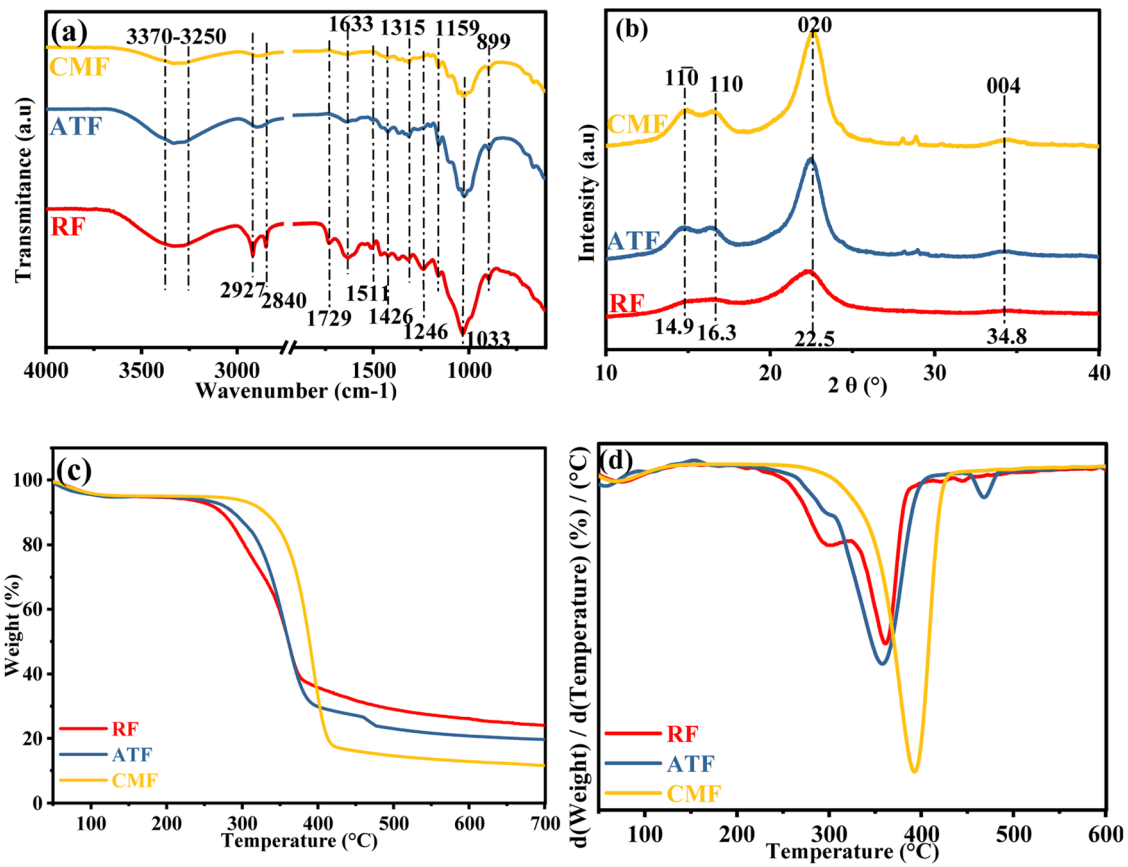

Fig. 2 (a) FTIR spectra, (b) XRD pattern, (c) TGA and (d) DTG curve of RF, ATF and CMF.

© 2023 The Author(s). Published by the Royal Society of Chemistry

undergoes a two-step degradation which is confirmed by the presence of two peaks in the DTG curve, the first degradation occurred at 279 °C and the second one at 340 °C, the first degradation is attributed to the decomposition of hemicellulose and lignin, the second degradation is attributed to the decomposition of cellulose. It's noteworthy to mention that the degradation of the ATF and CMF samples follows an almost identical degradation behaviour, as shown in TGA and DTG curve, indicating that most of the hemicellulose and lignin were removed after the alkali and bleaching treatment.[48]

SEM was used to analyse the morphology of RF, ATF, and CMF. Fig. 3 demonstrates significant changes in RF after the alkali treatment and bleaching. Untreated RF Fig. 3(a) exhibited a strongly bounded fiber with rough compact surface, whereas ATF appears separated into bundled individual micro-sized structures in Fig. 3(b). In Fig. 3(c), single microfibers with a clean and smooth surface are individualized. The changes in the fiber morphology indicate that the hemicellulose and lignin were successfully removed during the chemical treatments.

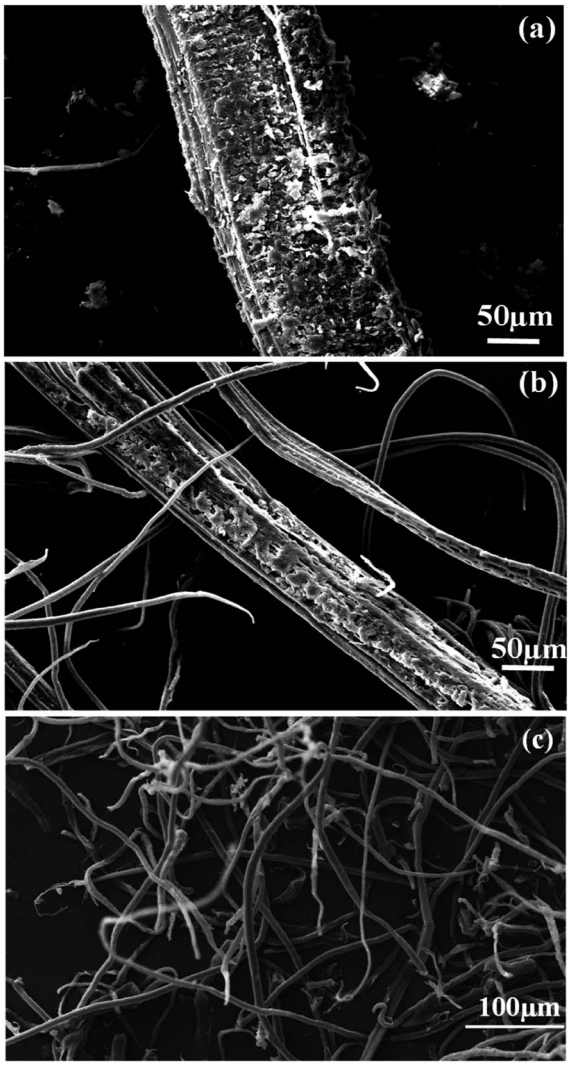

Fig. 3 SEM images of (a) RF, (b) ATF and (c) CMF.

3.1.2. Clay and composite characterization. ca-Gh composite has been prepared simply, which molecular structure was characterized by XRD, zeta-potential, BET, EDX and SEM to provide a theoretical basis for subsequent adsorption experimental results. According to the XRD patterns of Gh and ca-Gh shown in Fig. 4(a), the raw clay appeared to be mainly composed of the clay mineral stevensite (S), with a distinctive peak at d_{001} = 15.27 Å. d_{hkl} was determined using the Bragg equation. The other peaks are attributed to the associated minerals quartz (Q) and dolomite (D), as previously reported.[49] The interfoliar space decrease as it was d_{001} = 15.27 Å and as a result to the thermal treatment it became d_{100} = 9.93 Å. The XRD pattern shows few major changes as a result of the heat treatment, such as the disappearance and the weakening of the Q and D peaks, also additional new peaks appear to signify dolomite breakdown. Peaks that correspond to $CaCO_3$ are formed by the carbonisation of CaO, which becomes relatively unstable after MgO is depleted.[50] Mohamed *et al.* also came to the same conclusion that dolomite beaks down into $CaCO_3$ and $MgCO_3$.[51]

The surface charge of an adsorbent material generally has the strongest effect on its effectiveness.[52] Therefore, the zeta potential was measured under various pH levels in order to determine the surface charge properties of Gh and ca-GH, as shown in Fig. 4(b). Due to the presence of SiO_2 groups, Gh and ca-Gh, both exhibit a negative charge over the whole pH range studied. The observed results show that the zeta-potential rose with pH value, indicating good electronegativity at higher pHs. Fig. 4(c) show the results of the adsorption/desorption isotherms from the BET analysis, it can be concluded from these results that both materials display the isotherm type II characteristics with hysteresis loops (type H3). This type of isotherm was also observed in other clay-based materials, which is resulted from the aggregates with macro/mesopores, even though only the initial monolayer–multilayer segment of the isotherm is reversible.[53] EDX results displayed in Fig. 4(d) reveals the elements present in the surface of Gh and ca-Gh, the oxygen, magnesium, silica and calcium are the main elements in the composition of the clay mineral stevensite, the carbon in ca-Gh is generated from the carbonized fibers of CMF during the pyrolysis process, the initial composition of the CMF was 25%, and considering the weight loss during the thermal treatment, the qualitative value given by the EDX of carbon was 15.72%.

The result of the X-ray fluorescence analysis is in Table 1 reveals the typical composition of clays, with high content of magnesium for Gh which is a stevensite. The high silica's compositional content is a synonym of the presence of free silica and the presence of carbonate is relevant.

According to the SEM images of ca-Gh in Fig. 5(a) and (b), we can notice that the surface of the material is extremely rough, additionally, we can see tiny particles formed which might have resulted from the exfoliation of Gh layers.[54] The surface mapping displayed in Fig. 5(c) and (d)–(h) reveals the presence of all the elements and each component (O, Si, Mg, Ca, C) by itself, respectively. The surface mapping allows to observe how

 © 2023 The Author(s). Published by the Royal Society of Chemistry

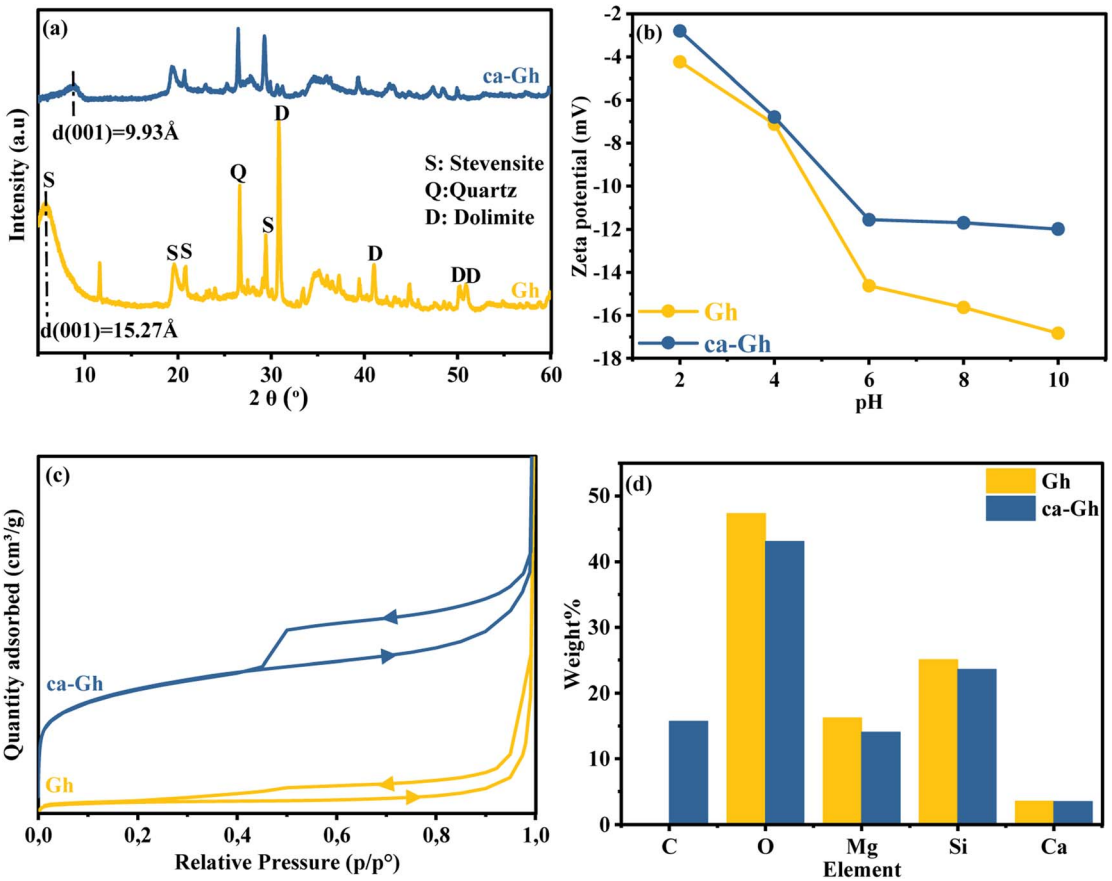

Fig. 4 (a) XRD pattern, (b) zeta potential, BET adsorption/desorption isotherm of Gh (c) and ca-Gh, and (d) EDX of Gh and ca-Gh.

Table 1 Chemical composition by XRF of Gh and ca-Gh

	Chemical composition (%)							
Clay minerals	SiO_2	Al_2O_3	SO_3	CaO	MgO	Fe_2O_3	K_2O	Other elements
Gh	62.48	1.77	2.38	17.20	10.51	2.72	1.20	1.29

these elements are distributed all over the composite's surface, it also enables to confirm that the carbon was successfully deposited on the surface without changing the essential elements of the composition of the clay. After carbonisation, the BET analysis revealed that the surface area of Gh increased significally, going from 88.31 $m^2\ g^{-1}$ to 164.97 $m^2\ g^{-1}$ for Gh and ca-Gh, respectively.

3.2. Adsorption study

3.2.1. pH effect. The pH value of the solution directly influences the adsorption capacity. As it can be noticed from Fig. 6(a), the quantity adsorbed for both adsorbents increased as the pH increased. According to the characterization of the ghassoul clay that have been done in this work, it was revealed that it is mainly composed of stevensite, quarts and dolomite. It is well known that the clay mineral surface has a net positive charge a pH value lower that it pH_{pzc} and a net negative charge at pH levels higher than its pH_{pzc}.[55] According to Benhammou's work,[49] the pH_{pzc} of Gh is 2, meaning that at pH values higher, the clay's surface is negatively charged. The reduced sorption at low pH is also possibly due to the competition of H^+ with the cations for the adsorption sites of the adsorbent, same behaviour was reported in previous studies.[49]

3.2.2. Temperature effect. The temperature of the solution is one of the factors that strongly influences the adsorption capacity. From Fig. 6(b), for Gh it can be noticed that the elimination rises with temperature as a result of an increase in metal ions mobility. Although for ca-Gh, this is not the case, which could be explained by the fact that the adsorption capacity has already reached its maximum. The values of the thermodynamic parameters are reported in Table 2. The fact that $\Delta G°$ is always negative for ca-Gh at all temperatures tested reveals that the Cd^{2+} adsorption is spontaneous, N. Mohammadi *et al.* also have found a negative charge.[1] The endothermic

© 2023 The Author(s). Published by the Royal Society of Chemistry

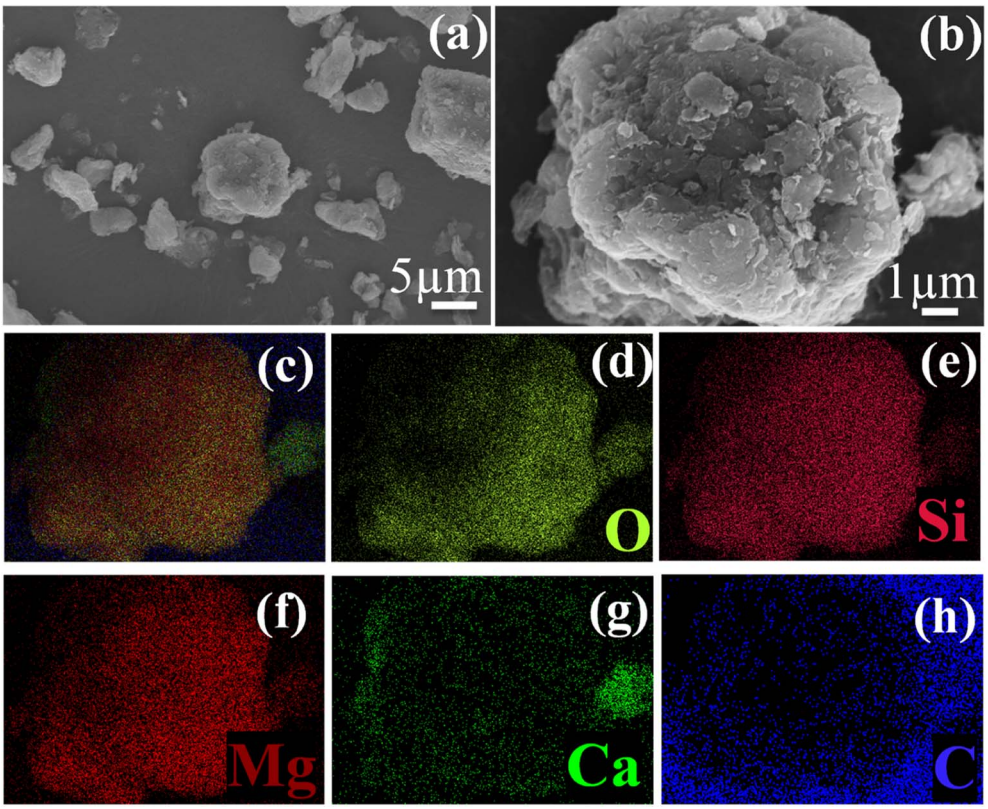

Fig. 5 (a and b) SEM images and (c–h) surface mapping of ca-Gh.

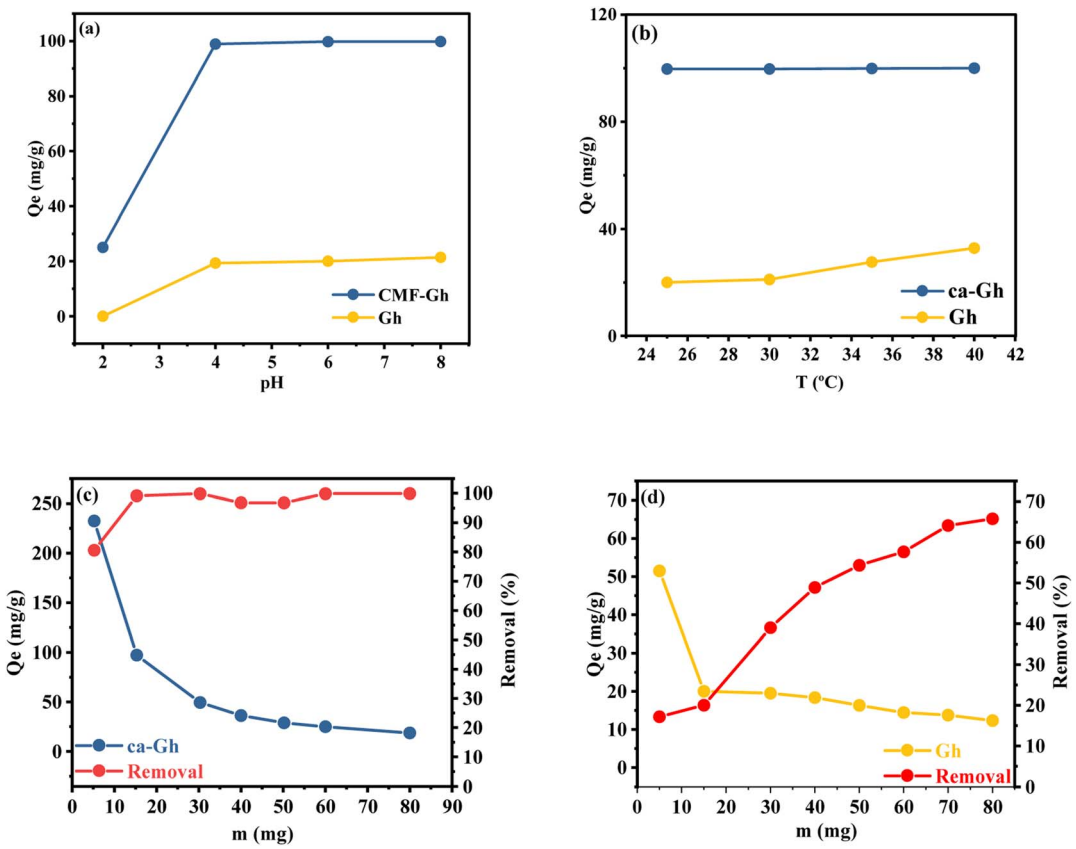

Fig. 6 (a) Effect of pH, (b) temperature and (c and d) dose of absorption of Cd^{2+} by Gh and ca-Gh.

 © 2023 The Author(s). Published by the Royal Society of Chemistry

Table 2 Thermodynamic parameters for Cd^{2+} adsorption onto Gh and ca-Gh at various temperatures

	$\Delta G°$ (J mol^{-1})					
Temperature	298.15 K	303.15 K	308.15 K	313.15 K	$\Delta H°$ (J mol^{-1})	$\Delta S°$ (J mol^{-1})
Gh	412.59	399.59	297.33	224.18	0.000024	0.000361
ca-Gh	−1684.14	−1759.12	−1989.34	−2378.19	0.000008	0.000445

nature of Cd^{2+} adsorption is supported by the decreasing $\Delta G°$ values with temperature which results in positive values for $\Delta H°$, which is also compatible with the fact that the removal is temperature-dependant. Additionally, the positive values of $\Delta S°$ support the adsorption process's favourable and spontaneous nature, which may be connected to an increase in randomness at the solid–liquid surface, M. Qhubu. *et al.* also have found a positive value of $\Delta S°$ which lead them to the same conclusion.[2]

3.2.3. Adsorbent masse effect. The outcome of varying the adsorbent mass from 5 to 80 mg were applied to study the effect of adsorbent dosage Fig. 6(c) and (d) while keeping the initial concentration of Cd^{2+} fixed (100 mg L^{-1}). It was found that when the adsorbent mass increases, the removal percentage considerably improves, going from 17.17% to 65.79% for Gh and from 80.61% to 99.91% for ca-Gh. For Gh, after 40 mg, the adsorption capacity did not significally increase, that can be explained by either the filling of nearly all the sites of the surface of our adsorbent or by inter-particle interactions caused by the agglomeration of the clay particles between them, as it was reported in this work.[16] In the case of ca-Gh, the adsorption capacity has almost reached its maximum after 15 mg, which may be concluded from the nearly complete removal of all the cadmium ions from the solution.

3.2.4. Time effect. The variation of adsorption capacity with increasing contact time was investigated. Fig. 7(a) shows that the amount of Cd^{2+} adsorbed on the two investigated adsorbents improves with increasing time until it reaches a maximum level of approximately 60 minutes. For Gh and ca-Gh respectively, the maximum uptake capacity adsorbed was 20.40 mg g^{-1} and 99.76 mg g^{-1}. For a better understanding of how the adsorption process takes place on the surface of the adsorbent, numerous kinetic models are available in the literature.[56–58] Two kinetic models, pseudo-first-order and pseudo-second-order were used to study the adsorption of Cd^{2+}

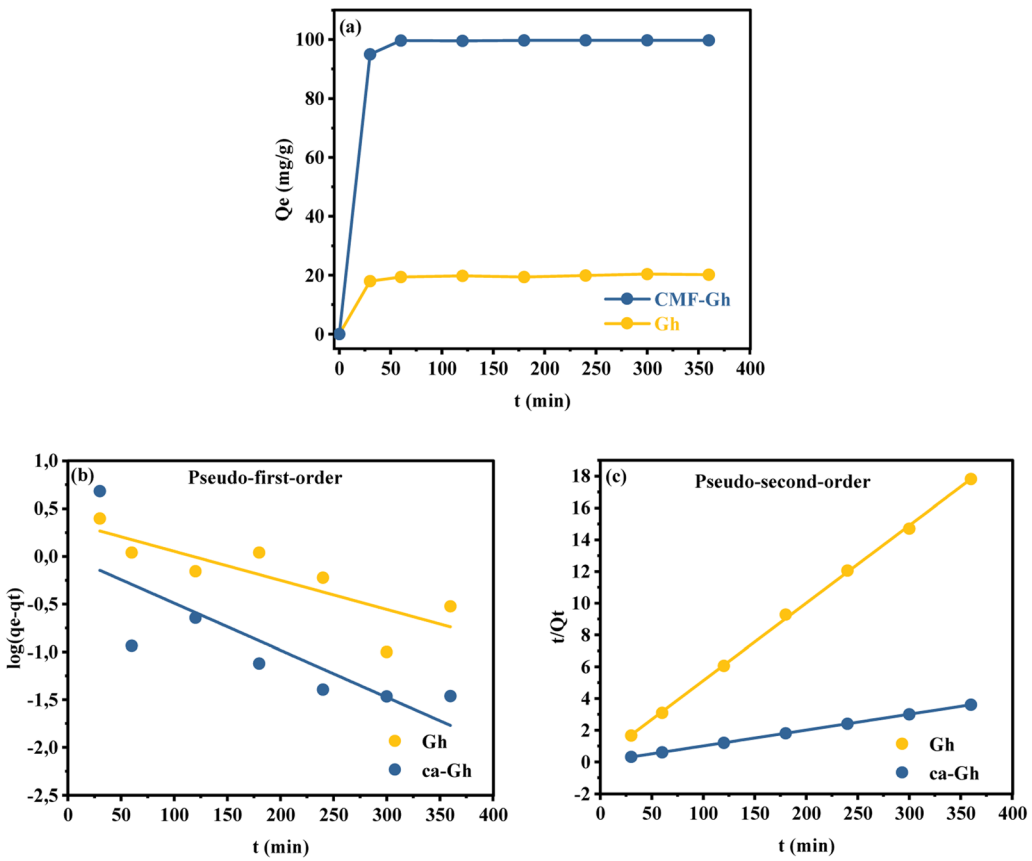

Fig. 7 (a) Experimental and (b and c) fitted data to two kinetic models for the adsorption of Cd^{2+} by Gh and ca-Gh.

© 2023 The Author(s). Published by the Royal Society of Chemistry

Table 3 Parameters of two kinetic models for Cd^{2+} adsorption by Gh and ca-GH

Kinetic model	Parameters	Gh	ca-Gh
Pseudo-first-order	K_1 (min^{-1})	0.003	0.005
	q_e ($mg\ g^{-1}$)	1.432	1.002
	R^2	0.691	0.628
Pseudo-second-order	K_2 ($g\ mg^{-1}\ min^{-1}$)	0.010	0.013
	q_2 ($mg\ g^{-1}$)	20.449	100.000
	R^2	0.999	0.999

ions in this study. Fig. 7(b) and (c) presents the linear plot of the experimental data, and Table 3 provides a summary of the parameter's estimated values. The pseudo-second-order model has a higher correlation coefficient for both adsorbents, according to the kinetic modelling results. The predicted uptake capacities of 20.45 mg g^{-1} and 100 mg g^{-1} for Gh and ca-Gh, respectively, were closer to those of the experimental data, with $R^2 = 0.9995$ and 1 for Gh and ca-Gh, respectively. We can assume that chemisorption is the mechanism behind the adsorption phenomenon.[59]

3.2.5. Concentration effect. Cd(II) ions were studied by mixing 15 mg of the adsorbent with 15 mL of Cd^{2+} solution at concentrations of 20, 40, 80, 100, 120, 160, 200, 500 and 600 mg L^{-1}. Syringe filters were used to filter suspensions once they had reached equilibrium. Fig. 8(a) illustrates how the initial metal concentration affects the efficiency of Gh and ca-Gh to remove Cd^{2+} ions from an aqueous solution. As it can be noticed the adsorbed quantities rise as the initial concentration rises especially for ca-Gh. This increase could be explained by the fact that the availability of Cd^{2+} ions and the progressive saturation of the adsorption sites available at the

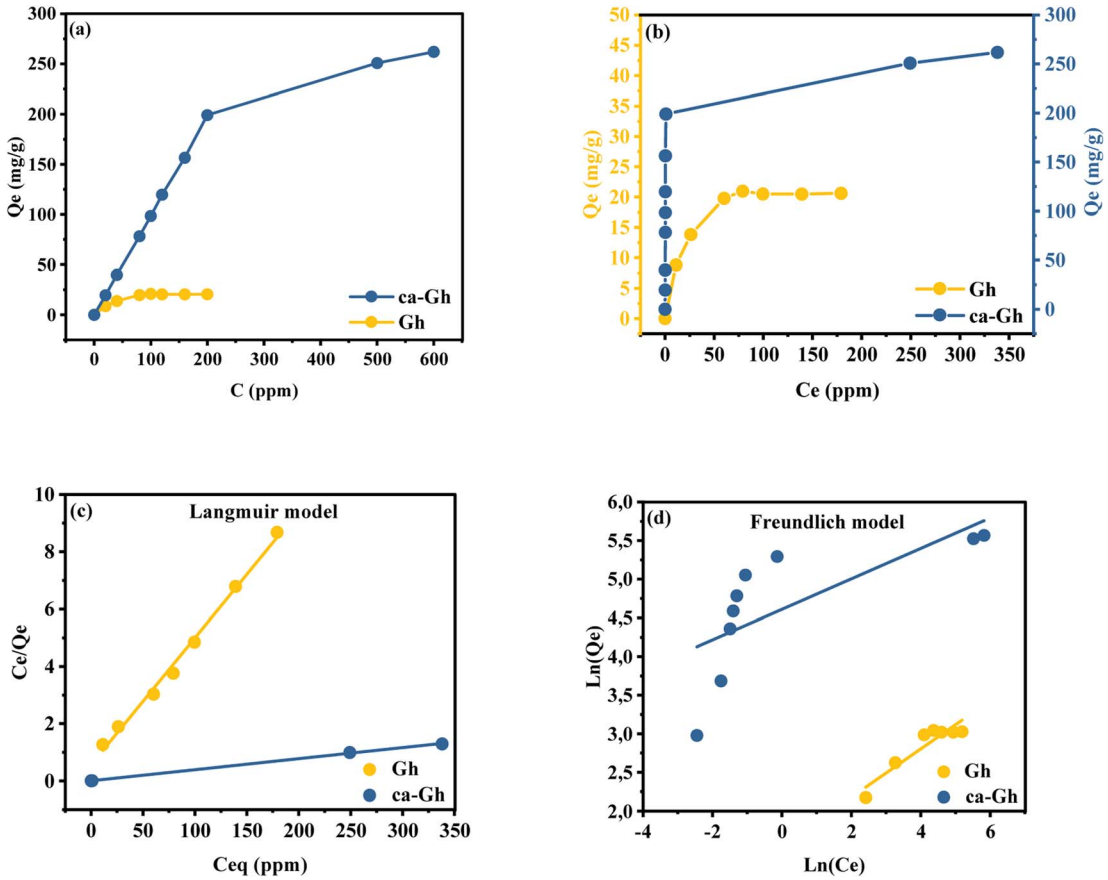

Fig. 8 (a) Experimental equilibrium, (b) isotherm, (c) linear fitting data to Langmuir and (d) Freundlich isotherm equation of Cd^{2+} adsorption of by Gh and ca-Gh.

Table 4 Parameters of Langmuir and Freundlich models for Cd^{2+} adsorption by Gh and ca-GH

Sample	Langmuir			Freundlich		
Parameters	Q_m ($mg\ g^{-1}$)	K_L ($L\ mg^{-1}$)	R^2	K_F ($mg\ g^{-1}$)	n	R^2
Gh	22.5734	0.0781	0.9941	4.7185	3.1949	0.8654
ca-Gh	256.4103	1.2581	0.9995	100.4800	5.0709	0.5173

 © 2023 The Author(s). Published by the Royal Society of Chemistry

Table 5 Adsorption capacities for Cd^{2+} using different adsorbents based on carbonaceous materials

Adsorbent	Q (mg g^{-1})	Ref.
Oxidized multiwalled carbon nanotube	23.40	63
Hydroxyapatite tailored hierarchical porous biochar composite	88.10	64
Carbonaceous material from pyrolyzed sewage sludge	15.00	65
Carbonaceous nanowire membrane	70.00	66
Carbonaceous composite	256.41	This study

surface of the adsorbent.[60,61] The clearance rates of Cd^{2+} for Gh and ca-Gh were 20.6 mg g^{-1} and 261.9 mg g^{-1}, respectively. The results of the isotherm Fig. 8(b) were fitted to Langmuir Fig. 8(c) and Freundlich Fig. 8(d) isotherm models. According to the Langmuir adsorption model, there is a saturated monolayer of adsorbate molecules at the surface of the adsorbent, which corresponds to a maximum limiting uptake.

On the other side, according to the Freundlich model, adsorption takes place on a heterogeneous surface using a multilayer adsorption mechanism, and the amount that is adsorbed rises in proportion to the concentration of molecules that are being adsorbed.[62]

As shown in Table 4, the correlation coefficients R^2 of the Langmuir model are higher and nearer to 1 for both adsorbents. Also, the fact that the values of n are higher than 1, indicates that the adsorption of Cd^{2+} is advantageous since this parameter describes the adsorption intensity. Furthermore, the estimated maximum adsorption capacities from Langmuir models are quite similar to those obtained experimentally. In this context, monolayer adsorption on a homogeneous surface is what we might refer to as the cadmium adsorption process into Gh and ca-Gh. The adsorption capacity of various materials described in literature is compiled in Table 5. Compared to the majority of the materials mentioned, the synthetized carbonaceous ghassoul has a high adsorption capacity.

4. Conclusion

In the present study, a natural Moroccan stevensite known as ghassoul, and cellulose microfibers isolated from Alfa fibers were used to synthetize a carbonaceous composite by pyrolysis. By employing alkali and bleaching treatments, pure CMF with a yield of 40% have been obtained from RF. The CMF, Gh and ca-Gh were characterized. Gh appeared to be mainly composed of stevensite. The carbon was deposed successfully and appeared to be well dispersed on the surface of the clay. The material appeared to be a powerful adsorbent for cadmium ions in aqueous media according to the adsorption values. The Langmuir isotherm model was best suited to simulate the cadmium adsorption on the synthetized composite. Monolayer adsorption on homogeneous surfaces appeared to be the adsorption mechanism. The experimentally determined maximal adsorption capacity was 261.9 mg g^{-1} for ca-Gh. In addition to the strong correlation coefficients, experimental kinetic data showed that the pseudo-second order model provides a good agreement between model fitting and experimentally equilibrium adsorption capacity. It can be concluded that the chemical process seemed to be in control of Cd^{2+} adsorption. Additionally, the thermodynamic characteristics indicated that the adsorption process is endothermic and spontaneous. In conclusion, the novel carbonaceous composite that was synthetized in this work is very efficient for the recovery of cadmium from aqueous media.

Conflicts of interest

There are no conflicts to declare.

Acknowledgements

The financial assistance of the Office Chérifien des Phosphates (OCP S.A.) in the Moroccan Kingdom toward this research is hereby acknowledged.

References

1 M. Thamarai Selvi and A. Zahir Hussain, *Mater. Today: Proc.*, 2022, **59**, 1349–1356.
2 Y. Aoulad El Hadj Ali, M. Ahrouch, A. Ait Lahcen, Y. Abdellaoui and M. Stitou, *Chem. Afr.*, 2022, **2022**, 1–30.
3 M. Ahrouch, J. M. Gatica, K. Draoui, D. Bellido and H. Vidal, *Chemosphere*, 2020, **259**, 127526.
4 R. El Kaim Billah, F. El Bachraoui, B. El Ibrahimi, H. Abou Oualid, Z. Kassab, G. Giácoman-Vallejos, M. Sillanpää, M. Agunaou, A. Soufiane and Y. Abdellaoui, *J. Solid State Chem.*, 2022, **310**, 123023.
5 G. H. Parker, C. E. Gillie, J. V. Miller, D. E. Badger and M. L. Kreider, *Toxicol. Rep.*, 2022, **9**, 238–249.
6 B. A. Fowler, *Toxicol. Appl. Pharmacol.*, 2009, **238**, 294–300.
7 M. Ahrouch, J. M. Gatica, K. Draoui, D. Bellido and H. Vidal, *Chemosphere*, 2020, **259**, 127526.
8 Q. Lin, G. Zeng, G. Yan, J. Luo, X. Cheng, Z. Zhao and H. Li, *Chem. Eng. J.*, 2022, **427**, 131668.
9 C. Y. P. Ayekoe, D. Robert and D. G. Lanciné, *Catal. Today*, 2017, **281**, 2–13.
10 M. Fasano, M. Morciano, L. Bergamasco, E. Chiavazzo, M. Zampato, S. Carminati and P. Asinari, *Appl. Energy*, 2021, **304**, 117661.
11 C. F. Z. Lacson, M. C. Lu and Y. H. Huang, *Chem. Eng. J.*, 2021, **415**, 128917.
12 M. Ahrouch, J. M. Gatica, K. Draoui, D. Bellido-Milla and H. Vidal, *Environ. Technol. Innovation*, 2022, **27**, 102765.
13 L. Bouna, A. A. El Fakir, A. Benlhachemi, K. Draoui, S. Villain and F. Guinneton, *Mater. Today: Proc.*, 2020, **22**, 22–27.

© 2023 The Author(s). Published by the Royal Society of Chemistry

14 R. El Kaim Billah, M. Aminul Islam, H. Lgaz, E. C. Lima, Y. Abdellaoui, Y. Rakhila, O. Goudali, H. Majdoubi, A. A. Alrashdi, M. Agunaou and A. Soufiane, *Arabian J. Chem.*, 2022, **15**, 104123.
15 Y. Abdellaoui, H. Abou Oualid, A. Hsini, B. El Ibrahimi, M. Laabd, M. El Ouardi, G. Giácoman-Vallejos and P. Gamero-Melo, *Chem. Eng. J.*, 2021, **404**, 126600.
16 A. Naboulsi, M. El Himri, E. K. Gharibi and M. El Haddad, *Surf. Interfaces*, 2022, **33**, 102227.
17 Z. Sun, J. Xu, G. Wang, A. Song, C. Li and S. Zheng, *Appl. Clay Sci.*, 2020, **184**, 105373.
18 Y. Abdellaoui, M. T. Olguín, M. Abatal, B. Ali, S. E. Díaz Méndez and A. A. Santiago, *Superlattices Microstruct.*, 2019, **127**, 165–175.
19 K. Elass, A. Laachach, A. Alaoui and M. Azzi, *Appl. Clay Sci.*, 2011, **54**, 90–96.
20 Y. El Mouzdahir, A. Elmchaouri, R. Mahboub, A. ElAnssari, A. Gil, S. A. Korili and M. A. Vicente, *Appl. Clay Sci.*, 2007, **35**, 47–58.
21 A. Naboulsi, M. El Himri, E. K. Gharibi and M. El Haddad, *Surf. Interfaces*, 2022, **33**, 102227.
22 K. Elass, A. Laachach, A. Alaoui and M. Azzi, *Appl. Clay Sci.*, 2011, **54**, 90–96.
23 M. Ahrouch, J. M. Gatica, K. Draoui, D. Bellido-Milla and H. Vidal, *Environ. Technol. Innovation*, 2022, **27**, 102765.
24 A. Benhammou, A. Yaacoubi, L. Nibou and B. Tanouti, *J. Colloid Interface Sci.*, 2005, **282**, 320–326.
25 Y. El Mouzdahir, A. Elmchaouri, R. Mahboub, A. ElAnssari, A. Gil, S. A. Korili and M. A. Vicente, *Appl. Clay Sci.*, 2007, **35**, 47–58.
26 X. Wang, X. Li, L. Peng, S. Han, C. Hao, C. Jiang, H. Wang and X. Fan, *Chemosphere*, 2021, **279**, 130504.
27 S. Chaouf, S. El Barkany, H. Amhamdi, I. Jilal, Y. El Ouardi, M. Abou-salama, M. Loutou, A. El-Houssaine, H. El Ouarghi and A. El Idrissi, *Mater. Today: Proc.*, 2020, **31**, S175–S182.
28 M. H. Salim, Z. Kassab, E. Ablouh, H. Sehaqui, A. Aboulkas, R. Bouhfid, A. E. K. Qaiss and M. El Achaby, *Int. J. Biol. Macromol.*, 2022, **200**, 182–192.
29 E.-H. Ablouh, Z. Kassab, F. Semlali Aouragh Hassani, M. El Achaby and H. Sehaqui, *RSC Adv.*, 2022, **12**, 1084–1094.
30 E.-H. Ablouh, R. Jalal, M. Rhazi and M. Taourirte, *Int. J. Biol. Macromol.*, 2020, **151**, 492–498.
31 B. G. Fouda-Mbanga, E. Prabakaran and K. Pillay, *Biotechnol. Rep.*, 2021, **30**, e00609.
32 E. Ablouh, A. Essaghraoui, N. Eladlani, M. Rhazi and M. Taourirte, *Water Environ. Res.*, 2019, **91**, 239–249.
33 N. Eladlani, E. M. Dahmane, E. Ablouh, A. Ouahrouch, M. Rhazi, M. Taourirte and M. Neffa, *J. Water Chem. Technol.*, 2019, **41**, 175–181.
34 E. Ablouh, Z. Hanani, N. Eladlani, M. Rhazi and M. Taourirte, *Sustainable Environ. Res.*, 2019, **29**, 5.
35 S. Chaouf, S. El Barkany, H. Amhamdi, I. Jilal, Y. El Ouardi, M. Abou-salama, M. Loutou, A. El-Houssaine, H. El Ouarghi and A. El Idrissi, *Mater. Today: Proc.*, 2020, **31**, S175–S182.
36 Z. Kassab, Y. Abdellaoui, M. H. Salim and M. El Achaby, *Mater. Lett.*, 2020, **280**, 128539.
37 M. H. Salim, Y. Abdellaoui, A. Ait Benhamou, E. H. Ablouh, M. el Achaby and Z. Kassab, *Cellulose*, 2022, **29**, 5117–5135.
38 D. S. Tong, C. W. Wu, M. O. Adebajo, G. C. Jin, W. H. Yu, S. F. Ji and C. H. Zhou, *Appl. Clay Sci.*, 2018, **161**, 256–264.
39 N. E. Mousa, C. M. Simonescu, R. E. Pătescu, C. Onose, C. Tardei, D. C. Culiță, O. Oprea, D. Patroi and V. Lavric, *React. Funct. Polym.*, 2016, **109**, 137–150.
40 K. L. Tan and B. H. Hameed, *J. Taiwan Inst. Chem. Eng.*, 2017, **74**, 25–48.
41 K. Y. Foo and B. H. Hameed, *Chem. Eng. J.*, 2010, **156**, 2–10.
42 M. El Achaby, Z. Kassab, A. Barakat and A. Aboulkas, *Ind. Crops Prod.*, 2018, **112**, 499–510.
43 F.-Z. El Bouchtaoui, E.-H. Ablouh, I. Kassem, Z. Kassab, H. Sehaqui and M. El Achaby, *J. Coat. Technol. Res.*, 2022, **19**, 1551–1565.
44 Z. Kassab, A. Boujemaoui, H. Ben Youcef, A. Hajlane, H. Hannache and M. El Achaby, *Cellulose*, 2019, **26**, 9567–9581.
45 A. Bahloul, Z. Kassab, F. Aziz, H. Hannache, R. Bouhfid, A. E. K. Qaiss, M. Oumam and M. El Achaby, *Cellulose*, 2021, **28**, 4089–4103.
46 D. Watkins, M. Nuruddin, M. Hosur, A. Tcherbi-Narteh and S. Jeelani, *J. Mater. Res. Technol.*, 2015, **4**, 26–32.
47 F.-Z. El Bouchtaoui, E.-H. Ablouh, M. Mhada, I. Kassem, M. H. Salim, S. Mouhib, Z. Kassab, H. Sehaqui and M. El Achaby, *Int. J. Biol. Macromol.*, 2022, **221**, 398–415.
48 D. Watkins, M. Nuruddin, M. Hosur, A. Tcherbi-Narteh and S. Jeelani, *J. Mater. Res. Technol.*, 2015, **4**, 26–32.
49 A. Benhammou, A. Yaacoubi, L. Nibou and B. Tanouti, *J. Colloid Interface Sci.*, 2005, **282**, 320–326.
50 Y. T. Algoufi, G. Kabir and B. H. Hameed, *J. Taiwan Inst. Chem. Eng.*, 2017, **70**, 179–187.
51 M. A. Harech, M. Mesnaoui, Y. Abouliatim, Y. Elhafiane, A. Benhammou, A. Abourriche, A. Smith and L. Nibou, *Bol. Soc. Esp. Ceram. Vidrio*, 2021, **60**, 194–204.
52 E. H. Ablouh, Z. Kassab, F. Z. Semlali Aouragh Hassani, M. El Achaby and H. Sehaqui, *RSC Adv.*, 2022, **12**, 1084–1094.
53 K. S. W. Sing and R. T. Williams, *Adsorpt. Sci. Technol.*, 2004, **22**, 773–782.
54 D. S. Tong, C. W. Wu, M. O. Adebajo, G. C. Jin, W. H. Yu, S. F. Ji and C. H. Zhou, *Appl. Clay Sci.*, 2018, **161**, 256–264.
55 H. Moussout, H. Ahlafi, M. Aazza, R. Chfaira and C. Mounir, *Heliyon*, 2020, **6**(3), e03634.
56 N. Dobe, D. Abia, C. Tcheka, J. P. N. Tejeogue and M. Harouna, *Chem. Phys. Lett.*, 2022, **801**, 139707.
57 I. M'barek, H. Slimi, A. K. D. AlSukaibi, F. Alimi, R. H. Lajimi, L. Mechi, R. Ben Salem and Y. Moussaoui, *Arabian J. Chem.*, 2022, **15**, 103679.
58 Y. Abdellaoui, B. El Ibrahimi, H. Abou Oualid, Z. Kassab, C. Quintal-Franco, G. Giácoman-Vallejos and P. Gamero-Melo, *Chem. Eng. J.*, 2021, **421**, 129909.
59 C. A. Cimá-Mukul, Y. Abdellaoui, M. Abatal, J. Vargas, A. A. Santiago and B. Zambrano, *Bioinorg. Chem. Appl.*, 2019, 1–13.
60 Y. Sun, Y. Yu, S. Zhou, K. J. Shah, W. Sun, J. Zhai and H. Zheng, *Sep. Purif. Technol.*, 2022, **282**, 120002.

 © 2023 The Author(s). Published by the Royal Society of Chemistry

61 N. Dobe, D. Abia, C. Tcheka, J. P. N. Tejeogue and M. Harouna, *Chem. Phys. Lett.*, 2022, **801**, 139707.
62 I. M'barek, H. Slimi, A. K. D. AlSukaibi, F. Alimi, R. H. Lajimi, L. Mechi, R. Ben Salem and Y. Moussaoui, *Arabian J. Chem.*, 2022, **15**, 103679.
63 M. Šolić, S. Maletić, M. K. Isakovski, J. Nikić, M. Watson, Z. Kónya and S. Rončević, *J Environ. Chem. Eng.*, 2021, **9**, 105402.
64 W. Wu, Z. Liu, M. Azeem, Z. Guo, R. Li, Y. Li, Y. Peng, E. F. Ali, H. Wang, S. Wang, J. Rinklebe, S. M. Shaheen and Z. Zhang, *J. Hazard. Mater.*, 2022, **437**, 129330.
65 E. Gutiérrez-Segura, M. Solache-Ríos, A. Colín-Cruz and C. Fall, *J. Environ. Manage.*, 2012, **97**, 6–13.
66 Y.-J. Zhong, S.-J. You, X.-H. Wang, X. Zhou, Y. Gan and N.-Q. Ren, *Chem. Eng. J.*, 2013, **226**, 217–226.

© 2023 The Author(s). Published by the Royal Society of Chemistry